

RESEARCH ARTICLE

10.1002/2014JC010322

Key Points:

- Model well reproduces surge magnitude and surface cooling
- Surge is associated with continental shelf wave
- Cooling is dominated by direct wind mixing

Correspondence to:

G. Han,
Guoqi.Han@dfo-mpo.gc.ca

Citation:

Ma, Z., G. Han, and B. de Young (2015), Oceanic responses to Hurricane Igor over the Grand Banks: A modeling study, *J. Geophys. Res. Oceans*, 120, 1276–1295, doi:10.1002/2014JC010322.

Received 17 JUL 2014

Accepted 12 JAN 2015

Accepted article online 21 JAN 2015

Published online 25 FEB 2015

Oceanic responses to Hurricane Igor over the Grand Banks: A modeling study

Zhimin Ma¹, Guoqi Han², and Brad de Young¹

¹Department of Physics and Physical Oceanography, Memorial University of Newfoundland, St. John's, Newfoundland, Canada, ²Biological and Physical Oceanography Section, Fisheries and Oceans Canada, Northwest Atlantic Fisheries Centre, St. John's, Newfoundland, Canada

Abstract A three-dimensional (3-D) baroclinic finite-volume ocean model (FVCOM) was developed to examine the oceanic response to Hurricane Igor over the Grand Banks of Newfoundland. Hurricane Igor generated a storm surge of almost 1 m at St. John's and about 0.8 m at three nearby coastal tide gauge stations (Bonavista, Argentia and St. Lawrence). The surge magnitude from the 3-D baroclinic model agrees approximately with tide-gauge observations at all four stations, slightly better than that from an alternative 3-D barotropic case. The sudden drop of sea surface temperature caused by the storm, approximately 6°C as observed by buoys, is well simulated by the baroclinic model with a $k-\epsilon$ turbulence closure. A sensitivity simulation with the Mellor-Yamada turbulence closure significantly underestimates sea surface cooling. It is shown that the sea surface cooling is mainly associated with turbulent mixing, and to a lesser degree with Ekman upwelling. The model solution shows that the largest surge occurred between Bonavista and St. John's. Further analysis suggests the generation of a free continental shelf wave after the storm made land-fall, with the peak surge propagating from St. John's to St. Lawrence.

1. Introduction

The Grand Banks of Newfoundland, located in the northwest of the Atlantic Ocean, extend nearly 500 km wide and 600 km long of the midlatitude. Situated southeast of Newfoundland, the Banks are separated from it by the Avalon Channel (Figure 1). With the influence of different water masses, the cold fresh Labrador Current and the warm salty Gulf Stream, the shallow Grand Banks play an important role in regional climate variability and marine ecosystem function.

Occasionally from August to October, hurricanes or tropical storms passing over the Banks cause a storm surge, along with drops in sea surface temperature (SST) and enhancement in vertical mixing. On 21 September 2010, Hurricane Igor, the most intense hurricane in Newfoundland in recent decades [Pasch and Kimberlain, 2011], hit this area, crossed over the Newfoundland Shelf, heading north into the Labrador Sea. SST observations on the Grand Banks showed a sharp decrease of 6°C [Han et al., 2012a]. Two strong storm surges were captured at the St. John's tide gauge station with a time difference of 11 h [Han et al., 2012b]. The occurrence of a phytoplankton bloom over the Banks was thought to be attributed to the mixed-layer deepening and upwelling associated with the strong wind [Han et al., 2012a].

Historically, scientists have used observations to explore the physical mechanisms of the oceanic response over the Newfoundland Shelf to the storm forcing. With wavelet and cross-wavelet analyses, Thiebaut and Vennell [2010] analyzed a fast continental shelf wave with data observed from six tide-gauges located along the Newfoundland coast under hurricanes. Han et al. [2012b] using satellite altimetry and tide-gauge data studied storm surges off Newfoundland caused by Hurricane Igor. They found that the storm surge was associated with a continental shelf wave generated by Hurricane Igor. However, monitoring both spatially and temporally the effects of hurricanes and tropical storms over the Grand Banks is limited, because there are few direct observations. Therefore, ocean modeling has become increasingly important to improve our understanding of the physical and biological response to extreme weather events in such under-observed regions.

Modeling studies of hurricane impacts on storm surge and the upper ocean's responses in coastal waters have been frequent over the past decade. [e.g., Resio and Westerink, 2008; Shen et al., 2006; Weisberg and

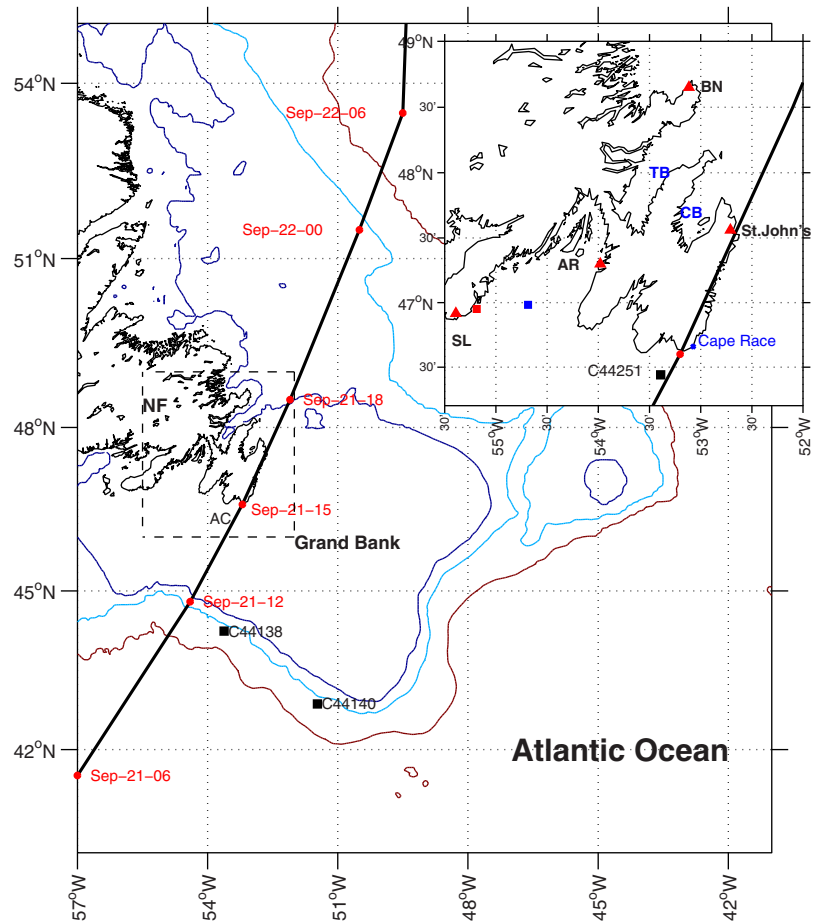


Figure 1. Hurricane Igor track (black thick line) and bathymetry (200, 1000, and 3000 m) over the Newfoundland Shelf. Tide-gauge stations (red triangles) include St. John's, Bonavista (BN), Argentia (AR) and St. Lawrence (SL). Locations of buoys are depicted in black (for temperature) and blue (for currents) squares. TB and CB indicate the Trinity Bay and Conception Bay, separately. AC is the Avalon Channel. Red square is the location where the model current and sea level are shown in Figure 15.

Zheng, 2006a, 2006b; Westerink et al., 2008]. Weisberg and Zheng [2006a, 2006b, 2008] and Rego and Li [2010] investigated the coastal inundation and surge propagation along a coastal embayment. Xie et al. [2004] discussed inundation algorithms and flooding velocities using the Princeton Ocean Model forced by an idealized Category-3 hurricane. Shen et al. [2006] simulated Hurricane Floyd's storm tide of September 1999 in Chesapeake Bay, with a substantial data set for validation and concluded that water levels inside the bay can be explained by the superposition of offshore surge propagation into the bay and local wind forcing. Focusing on the Newfoundland Shelf, deYoung and Tang [1990] discussed and modeled baroclinic near-inertial currents on the Grand Banks induced by a storm using a two layer idealized model. Using a linear barotropic model, Tang et al. [1998] investigated four types of wave motions with a barotropic response for an idealized moving storm off Newfoundland and Labrador. Mercer et al. [2002] modeled the barotropic response to a storm, determining the mechanism for a storm-generated wave effect on coastal sea level associated with a fast moving storm passing over the Grand Banks. However, these modeling studies were based on an idealized storm case and with an idealized barotropic formulation. Sheng et al. [2006] modeled upper ocean response to Hurricane Juan over the Scotia Shelf using a three-dimensional (3-D) baroclinic model. The sea surface cooling was reproduced reasonably well but the storm surge was not.

Most of the above studies are based on either two-dimensional (2-D) depth averaged model or a 3-D barotropic model. Weisberg and Zheng [2008] showed an improvement of storm surge simulation in their 3-D barotropic model over a 2-D depth-averaged model in the Tampa Bay, Florida. From our knowledge, studies

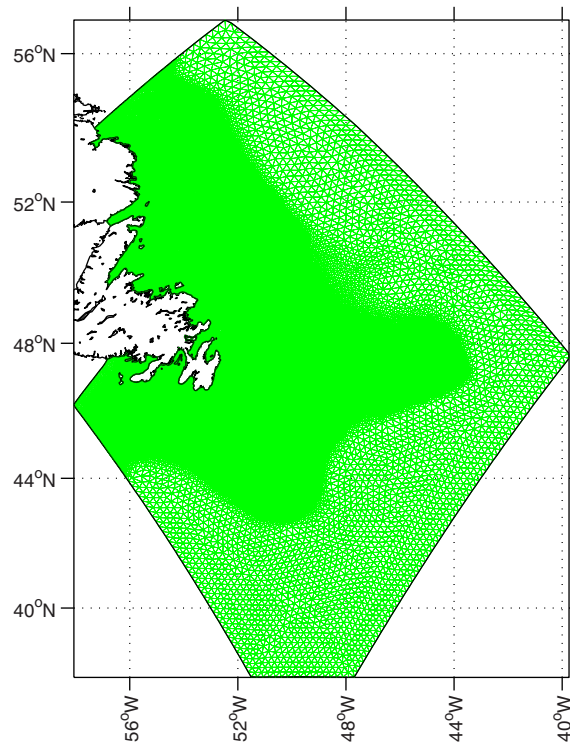


Figure 2. Mesh with 33863 nodes over the Newfoundland Shelf and Grand Banks. The resolution is around 1–2 km along the coastal and shelf edge. The Shelf and Banks are covered by 5 km unstructured triangular.

the storm and their sensitivity to model dynamics, parameterization and forcing. Finally, in section 5, we will present the summary and conclusions.

2. Circulation Models, Forcing, Initial and Open Boundary Conditions

2.1. FVCOM (3.1) Ocean Circulation Model and Mesh

The FVCOM model [Chen *et al.*, 2003] used in this study combines the advantages of horizontal grid flexibility and computational efficiency. Thus, this model is highly suitable for the present study area with an irregular complex coast line, reaching from shallow waters to the steep topography of the shelf break. A hybrid s -coordinate is chosen to better resolve the surface isopycnal layers and bottom topography [Chen *et al.*, 2011]. To account for the effect of atmospheric pressure on sea level, an atmospheric pressure gradient term is added into the momentum equation. A k - ϵ second-order turbulence model from General Ocean Turbulence Model (GOTM; available at <http://www.gotm.net>) is used in the present study. No normal flow to solid boundaries is applied at the lateral boundaries.

The storm surge effect is forced directly by wind stress and atmospheric pressure, but also is influenced by the continental shelf geometry and bathymetry. Thus, any storm simulation should include a domain large enough to contain the meteorological forcing fields and remote effects through coastally trapped wave propagation. The current model domain covers the southern Labrador Shelf including the Grand Banks, Newfoundland Shelf and the adjacent deep ocean (Figure 1). With 33,863 unequally spaced nodes and 64,480 elements, the horizontal resolution is typically 5 km over the shelf and 1–2 km along the coast and shelf edge (Figure 2). Vertically, 41 levels are nonuniformly distributed with a transition depth of 80 m. The first layer depth is within 1 m of the surface both for the shelf areas and the deep ocean. We use topography from the Canadian Hydrographic Service for the shelf part and etopo5 for the deeper ocean (www.ngdc.noaa.gov). The bathymetry has been smoothed to minimize the pressure gradient errors [Mellor *et al.*, 1993] with a volume conserving technique within each triangle. This technique limits the depth difference for three vertices at each triangle [Foreman *et al.*, 2009]. On the basis of Courant-Friedrichs-Levy (CFL)

on coastal ocean's response to hurricanes based on 3-D baroclinic models are limited. In this study, we will apply a state-of-the-art finite-volume coastal ocean model (FVCOM) [Chen *et al.*, 2003] to understand the baroclinic ocean responses to Hurricane Igor over the Grand Banks. Our main objectives are (1) to establish a 3-D high resolution baroclinic ocean model that can realistically simulate storm-induced oceanic responses and (2) to investigate features of storm surge, sea surface cooling and mixed-layer deepening and impacts of baroclinicity and turbulence parameterization. In section 2, we will describe the model setup, boundary conditions, forcing data, initial conditions and solution procedure. Section 3 will present comparisons between the model and observations and further describe circulation and hydrography. Section 4 discusses the mechanisms underlying storm surge and sea surface cooling associated with

numerical stability condition, model equations are solved with an integration time step of 1 s for the external mode and an internal to external mode ratio of 10.

2.2. Forcing and Hurricane Igor Wind Model

The model is forced by winds, heat fluxes and air pressure at the sea surface. We used spatially variable wind stress, air pressure, relative humidity, cloud cover, air temperature, dew point temperature and short-wave heat flux from NOAA/OAR/ESRL PSD, Boulder, Colorado, USA, (www.esrl.noaa.gov/psd) over the entire computational domain. The North American Regional Reanalysis (NARR) project is an extension of the NCEP Global Reanalysis which is run over the North American Region. The NARR model uses the very high resolution NCEP Eta Model (32 km/45 layer) together with the Regional Data Assimilation System (RDAS), with output 8 times daily. The heat flux data were calculated from MATLAB code including different functions to calculate the long-wave radiation, latent heat flux and sensible heat flux. A revised equation from *Li et al.* [2006] was used to calculate the albedo, including the white cap effect [*Monahan and MacNiocaill*, 1986], while modified code from the Tropical Ocean and the Global Atmospheric Program (TOGA)-Coupled Ocean Atmospheric Response Experiment (COARE) [*Fairall et al.*, 1996] was used to calculate the sensible and latent heat fluxes. The formulation of *Fung et al.* [1984] was used to estimate longwave radiation based on sea surface temperature from monthly mean temperature [*Geshelin et al.*, 1999] and air temperature, dew point temperature, cloud cover and wind speed.

Usually, the wind field generated from the atmospheric model substantially underestimates the maximum sustainable wind of a storm. A more effective way to create hurricane winds in storm surge modeling [e.g., *Peng et al.*, 2006a, 2006b; *Weisberg and Zheng*, 2008] is to reconstruct the wind field by fitting the analytical cyclone model from *Holland* [1980]. The radial distribution of wind relative to the storm centre and the maximum wind speed are specified such that:

$$V_H = \sqrt{\frac{B(P_{amb} - MCP)}{\rho_a} \left(\frac{RMW}{r}\right)^B \exp\left(-\frac{RMW}{r}\right) - \frac{rf}{2}} \quad (1)$$

$$V_{max} = \sqrt{\frac{B(P_{amb} - MCP)}{\rho_a e}} \quad (2)$$

Where r is the radial distance from the hurricane centre, V_H is the axisymmetric 1 min sustained wind speed as a function of the radius r , ρ_a is the air density ($= 1.15 \text{ kg/m}^3$), P_{amp} and MCP are the ambient and minimum central atmospheric pressures, respectively, e is the natural base logarithm, RMW is the radius of maximum winds, V_{max} is the maximum sustained wind speed, and B determines the shape of the storm wind field, $1.0 < B < 2.5$. We use a constant value of 1.1 for B . A practical and approximate way of converting V_H to the 10 m winds is to multiply a constant factor [*Phadke et al.*, 2003]. Instead, here we used another approximate approach, i.e., fitting the Holland model directly to 10 m wind data. The wind representation was determined from the NOAA Igor tracking report [*Pasch and Kimberlain*, 2011] and 3 hourly forecasting data (www.nhc.noaa.gov/archive/2010/IGOR.shtml). The report provides storm centre location, pressure, maximum 10 m wind speed, and forecasting data including the 64 knot wind radius in four directions (NE, NW, SE, SW) every 3 h. Based on the above equations (1) and (2), we calculated the maximum wind radius in each direction using the 64 knot wind radius data with the centre location provided by the Igor summary [*Pasch and Kimberlain*, 2011]. Then, the averaged maximum wind radial distance in four directions was treated as the RMW to construct the horizontal wind fields, neglecting asymmetry. The RMW and V_{max} are further interpolated linearly to provide values every 1 h. Then 1 min axisymmetric winds are generated every hour. The axisymmetric wind is rotated for an inflow angle. The inflow angle was difficult to determine precisely. A common practice is to apply a constant inflow angle. *Tang et al.* [1998] used 35° as the inflow angle suggesting that it was too large near the storm centre. *Zhang and Uhlhorn* [2012] estimated the averaged inflow angle to be $22.6 \pm 2.2^\circ$ for the 10 m wind based on observations. In the current study, we selected 25° as the inflow angle based on these two studies. Figure 3 compares reconstructed 1 min wind speeds from different B values with 1 min observations at St. John's, Bonavista and Argentia. The winds with $B=1.1$ have the best agreement with observations. The 1 min sustained winds are also converted to 10 min winds by multiplying a factor of 0.89 as a sensitivity case.

The 1 min (baseline) and 10 min sustained winds from the hurricane model are further blended with the NARR winds as follows: hurricane model winds within one RMW , NARR winds outside 4 RMW , and distance-based linear transition between the former and the latter between one and four RMW s.

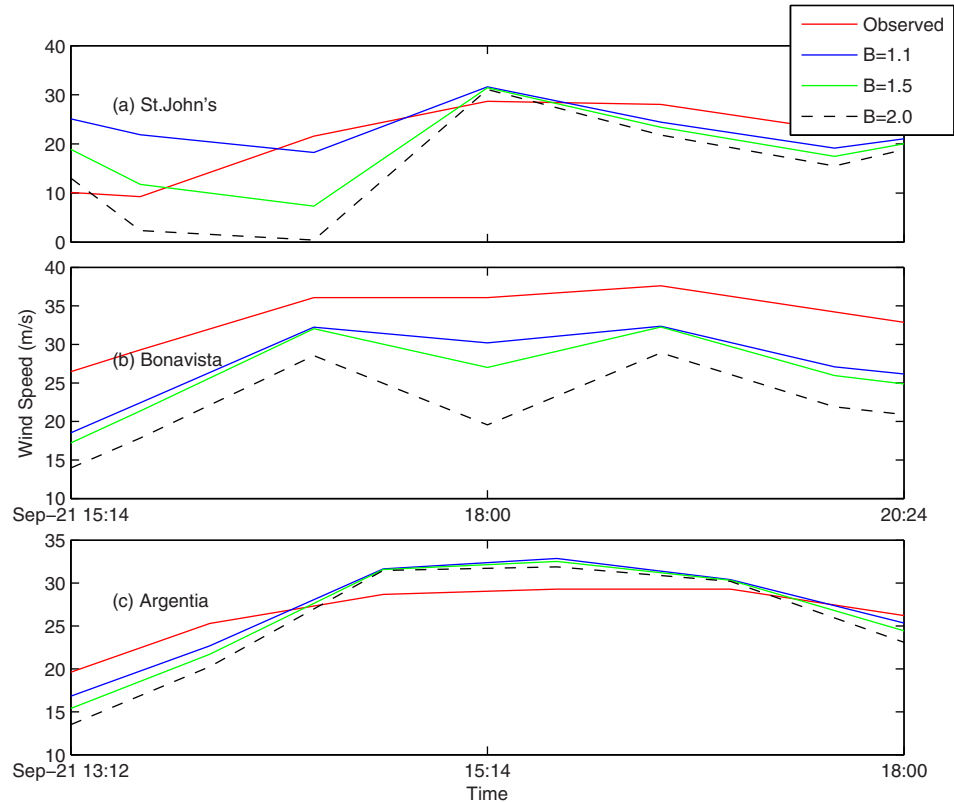


Figure 3. Comparison of 1 min sustained wind speeds reconstructed from the hurricane model using different B values with observations at St. John's, Bonavista, and Argentia.

Wind stress is computed every hour by:

$$\vec{\tau}_s = C_d \rho_a |\vec{\mathbf{V}}_w| \vec{\mathbf{V}}_w \quad (3)$$

where ρ_a is the air density, $\vec{\mathbf{V}}_w$ is the blended wind velocity, and C_d , a drag coefficient dependent on wind speed, is given by the *Large and Pond* [1981] formula of:

$$C_d \times 10^3 = 1.2 \left(\left| \vec{\mathbf{V}}_w \right| < = 11.0 \right)$$

$$C_d \times 10^3 = (0.49 + 0.065 \left| \vec{\mathbf{V}}_w \right|) (11 < = \left| \vec{\mathbf{V}}_w \right| < = 25)$$

$$C_d \times 10^3 = (0.49 + 0.065 \times 25) \left(\left| \vec{\mathbf{V}}_w \right| > = 25 \right)$$

2.3. Initial and Boundary Conditions

The model sea level and velocity were initialized from zero. The initial temperature and salinity conditions were generated from the historical monthly mean temperature and salinity data [Geshelin *et al.*, 1999] at standard z-levels. The model reaches an approximate dynamic equilibrium after running for 15 days. The model was integrated for 15 days with the July climatological condition and restarted from 1 August to 15 October 2010. The results from 1 September to 15 October were analyzed to examine the Igor influence over the upper ocean.

Tidal heights for the five major semi-diurnal (M_2, S_2 and N_2) and diurnal (K_1 and O_1) constituents based on Han *et al.* [2010] were specified along the open boundaries. Nontidal sea level at the lateral open boundaries was obtained from the climatological monthly mean solution of Han *et al.* [2008] and specified. The inverse barometric effect was adjusted at the open boundary [Jones and Davies, 2004; Sheng *et al.*, 2006].

The temperature and salinity along the open boundaries were interpolated from *Geshelin et al.*'s [1999] 1/6° by 1/6° climatological, monthly mean fields at each time step.

2.4. Model Validation Metrics

Besides commonly used correlation coefficient and root-mean-square (RMS) difference, another quantitative metric, the Willmott Score (WS) [Willmott, 1981], was used to evaluate the model sea level and sea surface temperature [e.g., Liu et al., 2009]. The WS is defined as:

$$WS = 1 - MSE / (|m - \langle o \rangle| + |o - \langle o \rangle|)^2 \quad (4)$$

where m and o represent modeled and observed variables respectively, $\langle o \rangle$ is the mean value of the observed variable, MSE is the mean square difference between model and observation. $WS = 1$ means the exact agreement, the closer to 1 the better agreement.

3. Model Validation

3.1. Tidal and Nontidal Sea Level

Harmonic constants of leading M_2 , S_2 , N_2 , K_1 and O_1 constituents derived from coastal tide gauges and bottom pressure gauges were obtained from *Han et al.* [2010]. Harmonic analysis including these five constituents and major over-tides (M_4 , M_6 , MS_4) was applied to the model solution from 1 September to 15 October 2010. For the five tidal constituents, the RMS error between observed data and model solution was 3.5 cm in amplitude and 8.3° in phase compared with 2.4 cm and 14.2° from *Han et al.* [2011]. The horizontal distributions (not shown) of five constituents are consistent with previous study and detailed description and figures could be found in *Han et al.* [2011]. Observed hourly sea levels were obtained from the Canadian Tides and Water Levels Data Archive (www.meds-sdmm.dfo-mpo.gc.ca/isdm-gdsi/twl-mne/index-eng.htm) at St. John's, Bonavista, Argentia, and St. Lawrence (Figure 1) for 2010. Harmonic analysis with 35 tidal constituents (including the aforementioned 8 constituents) was applied to detide-tide-gauge data [Pawlowicz et al., 2002]. The detided tide-gauge data were compared with the model results.

The results of hourly nontidal sea level were shown in Figure 4 (blue and red line), with the model mean sea level adjusted to match the observed relative to the chart datum over the period from day 264 to day 270. The inverse barometer effect was included. Simulated results agree well with observed water levels in these stations with a correlation coefficient above 0.9, including both storm-induced and other variability. During Hurricane Igor, sea level at these four stations, with the exception of Bonavista, showed two peaks. The first peak at St. John's was on year day 264, 15:30pm when the storm centre made landfall near Cape Race (see Figure 1), while the second one at this station was on year day 265, 02:30am when the storm centre traveled farther north, about 530 km northeast from St. John's (Figure 4). The second peak at St. Lawrence was 6–8 h later.

The RMS differences between the observed and simulated hourly values were averaged to be around 10 cm at the four tide-gauge stations, which nevertheless was relatively small compared to an average surge magnitude of 83 cm (Table 1). The averaged Willmott Score stayed as high as 0.90. The differences for the peak amplitude and timing were shown in Table 2. On average, the absolute amplitude difference was 8 cm (about 10% of the average surge magnitude) and the time lags were 1.3 h. Even though the model slightly over- or under-estimated the peak surge, it did capture the local surge's evolution and reproduce the low frequency sea level before and after the storm very well.

The model results at Argentia and St. Lawrence also show strong oscillations at a period of about 5 h (Figure 4). Placentia Bay has a longitudinal length of 130 km and an average depth of 125 m [Ma et al., 2012]. By treating it as horizontally triangular the natural oscillation period is estimated to be 5.4 h. Thus the strong short-period oscillations are probably associated with a storm-induced seiche. It is possible that the tide gauges did not capture the seiche well because of their locations. This also explains why the model peak surge is higher than the observed at the Argentia and St. Lawrence tide-gauge stations.

On year day 265, 02:40am, Jason-2 had a pass across the Grand Banks when the sea level was close to the second peak at St. John's. Model simulated sea level anomalies along the track were interpolated and compared with satellite observations from *Han et al.* [2012b] (Figure 5). Over the central Grand Banks (42°N–45.5°N), computed sea level captured the observations well. A sea level dip was found between

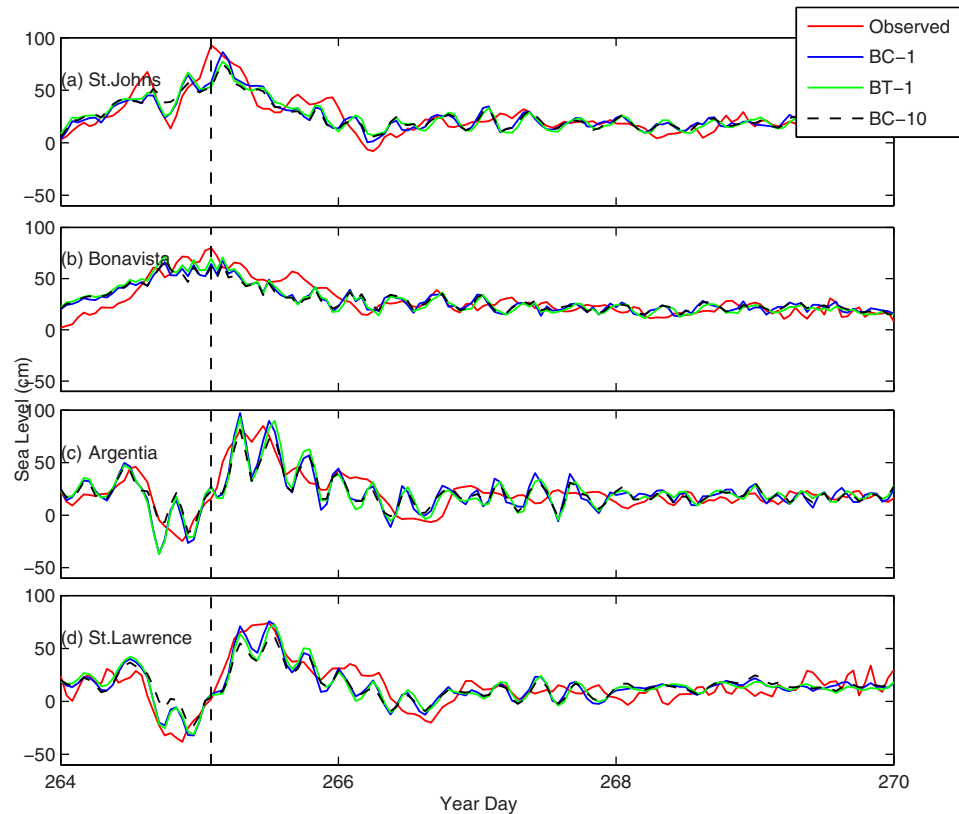


Figure 4. Hourly de-tided sea level anomalies from tide-gauge observations (red), 3-D baroclinic baseline model (BC-1, blue), 3-D barotropic case (BT-1, green) and 10 min sustained hurricane wind case (BC-10, black dash). Vertical black dashed line indicates the time of highest peak in St. John's.

44.5°N to 45.5°N both in the observations and the model results. However, a large sea level difference existed inshore (Figure 5b) due to the model delay of the peak at St. John's (Table 2). After 2 h, the model inshore elevation anomaly reached 0.6 m.

3.2. Sea Surface Temperature

The baseline model sea surface temperatures were compared with buoy measurements (<http://www.medsdmm.dfo-mpo.gc.ca/isdm-gdsi/waves-vagues/index-eng.htm>) in Figure 6 (blue and red line, respectively). One buoy (C44251) was deployed inshore and the other two were located along the shelf edge in the southern part of the Grand Banks (Figure 1). When the storm passed over, the sea surface temperature dropped by around 6°C. The simulated temperatures agree well with those observed. The correlation coefficients from day 264 to Day 270 were all above 0.9. The averaged RMS error between the observed and simulated temperature stayed around 1.6°C. The averaged Willmott Score was 0.83, indicating good agreement for both mean temperature and variability. The hurricane induced average temperature drop from the model was comparable to the observed drop within 1 °C . By comparing the temperature before and

Table 1. Validation Statistics Between Model and Observed Nontidal Sea Level Anomalies (cm)^a

Tide-Gauge Station	RMS Difference (cm)			Willmott Score (WS)		
	BC-1	BC-10	BT-1	BC-1	BC-10	BT-1
St. John's	9.5	10.5	10.2	0.91	0.88	0.90
Bonavista	9.1	9.9	9.2	0.90	0.87	0.90
Argentia	12.4	11.7	13.0	0.87	0.86	0.86
St. Lawrence	10.6	12.2	11.3	0.91	0.86	0.90
Mean Absolute	10.4	11.1	10.9	0.90	0.87	0.89

^aBC-1 is the baseline 3-D baroclinic model, BT is the 3-D barotropic case, and BC-10 is the 10 min sustained wind case.

Table 2. Storm Surge Peak Statistics (Model Minus Observations) for the Highest Peak^a

Tide-Gauge Station	Observed Peak Surge (cm)	Peak Difference (cm)			Peak Lag (h)		
		BC-1	BC-10	BT-1	BC-1	BC-10	BT-1
St. John's	94	-6	-18	-15	2	2	2
Bonavista	79	-12	-10	-8	2	2	2
Argentia	85	12	-3	8	2	2	2
St. Lawrence	75	2	-13	-2	0	0	1
Mean Absolute	83	8	11	8	1.5	1.5	1.8

^aBC-1 is the baseline 3-D baroclinic model, BT-1 is the 3-D barotropic case, and BC-10 is the 10 min sustained wind case.

after the storm, we found that the surface temperature did not return to the original level after the storm (Figure 6). In general, the net heat flux at the surface becomes weak for this region in late September. Therefore it is unlikely for the sea surface temperature to recover following passage of the storm. *Sheng et al.* [2006] simulated sea surface cooling of 3.5°C over the Scotian Shelf during Hurricane Juan. *Wada* [2005] reproduced sea surface cooling of 4°C south of Japan during Typhoon Rex.

3.3. Horizontal Temperature Distribution and Mixed Layer Depth

Figure 7 shows the 8 day averaged horizontal sea surface temperature distribution from the model and from satellite remote sensing data (pathfinder.nodc.noaa.gov) [Casey et al., 2010]. The 8 day periods are from 14 to 21 September and from 22 to 29 September, respectively. The satellite sea surface temperature was shown for the same time period. Before the storm, the satellite surface temperature showed an evident north-south gradient over the Grand Banks. The temperature was high, up to 20 °C in the south and low to 12 °C in the north. After the passage of the storm, the satellite surface temperature dropped significantly, around 6 °C over the Grand Banks but held a similar north-south gradient. Compared with the satellite temperature, similar spatial patterns before and after storm were clearly found from the model solutions. A large discrepancy between model results and satellite observations existed over the southern Grand Banks after the storm passed by. The model temperature is 14 °C while the satellite temperature is 11°C. The averaged mixed layer depth around the inshore buoy (C44251), calculated based on the model results (Figure 8), showed that the mixed layer deepened substantially following the passage of the storm, increasing from 19 m before the storm to around 27 m afterward. The mixed layer depth is defined as the depth where a density change of 0.125 kg m⁻³ from the sea surface value has occurred.

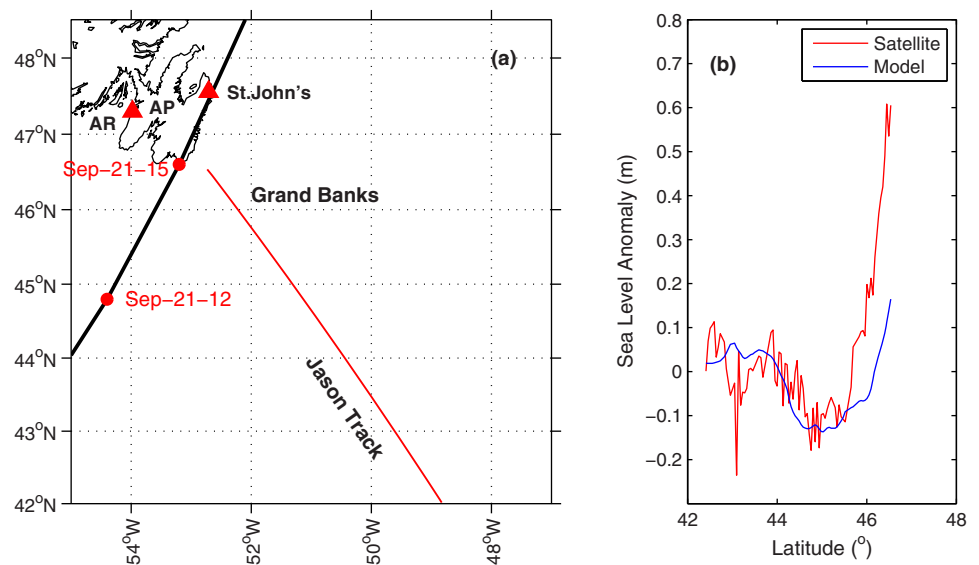


Figure 5. (a) Jason-2 satellite ground track (Red) and (b) sea level anomalies between model and satellite observations. Black thick line in (a) is the storm track. AP: Avalon Peninsula. AR: Argentia. Red triangles depict the location of tide gauge stations.

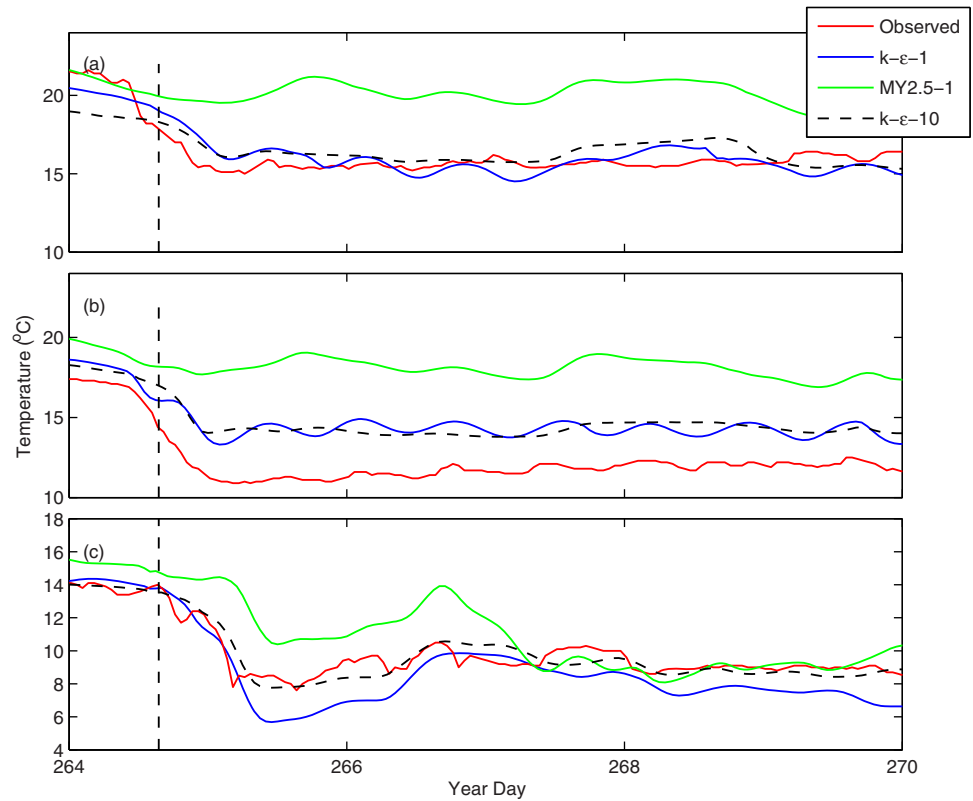


Figure 6. Hourly sea surface temperature from observation (red), baseline model with $k-\epsilon$ turbulence closure (blue), sensitivity case with MY2.5 (green), and sensitivity case with 10 min sustained hurricane winds (black dash) at (a) C44140, (b) C44138, and (c) C44251. Vertical black dashed line indicates the landfall time.

3.4. Surface Current

Surface currents were compared with observations at a station located in the mouth of Placentia Bay where buoy collected surface currents (0.5 m below the sea surface) are available. Half-hourly data were extracted from the Smart Bay Project (www.smartbay.ca). Data from 1 August to 31 December 2010 were de-tided for the 5 major constituents and 30 other minor constituents [Pawlowicz *et al.*, 2002] and smoothed with a 3 h low pass filter (Figure 9). In general, model calculated currents compare reasonably well with buoy observations especially during Hurricane Igor. From year day 264 to 266, surface current significantly increased to around 0.6 m/s and the direction changed suddenly from positive to negative (positive is eastward and northward). The peak currents were reached at year day 264, 19:55 when the storm centre moved to the northeast of Trinity Bay. Significant inertial oscillations were generated at a period of about 17 h. Detailed statistics were calculated between the observed and model currents. The RMS differences are 15 cm/s in both the eastward and northward components. Therefore, the model simulated the variability of surface current well during Hurricane Igor.

4. Discussion

4.1. Sensitivity Simulations Without Stratification, With Mellor-Yamada Turbulence Closure, or With 10 min Sustained Wind Forcing

Weisberg and Zheng [2008] found the importance of using a 3-D barotropic model instead of a 2-D depth-averaged one for storm surge in Tampa Bay, Florida. They attributed the 20% underestimation of surge in the 2-D model to the overestimation of bottom stress. Here we extend their work to examine the difference between our baseline 3-D baroclinic model and an alternative 3-D barotropic case (BT-1) while keeping wind forcing and sea level open boundary conditions the same. The results are shown in Figure 3, with detailed statistics in Tables 1 and 2. The 3-D barotropic model is almost as good as the baroclinic model in terms of the RMS difference and Willmott Score (Table 1). The statistics for the peak storm surge shows the

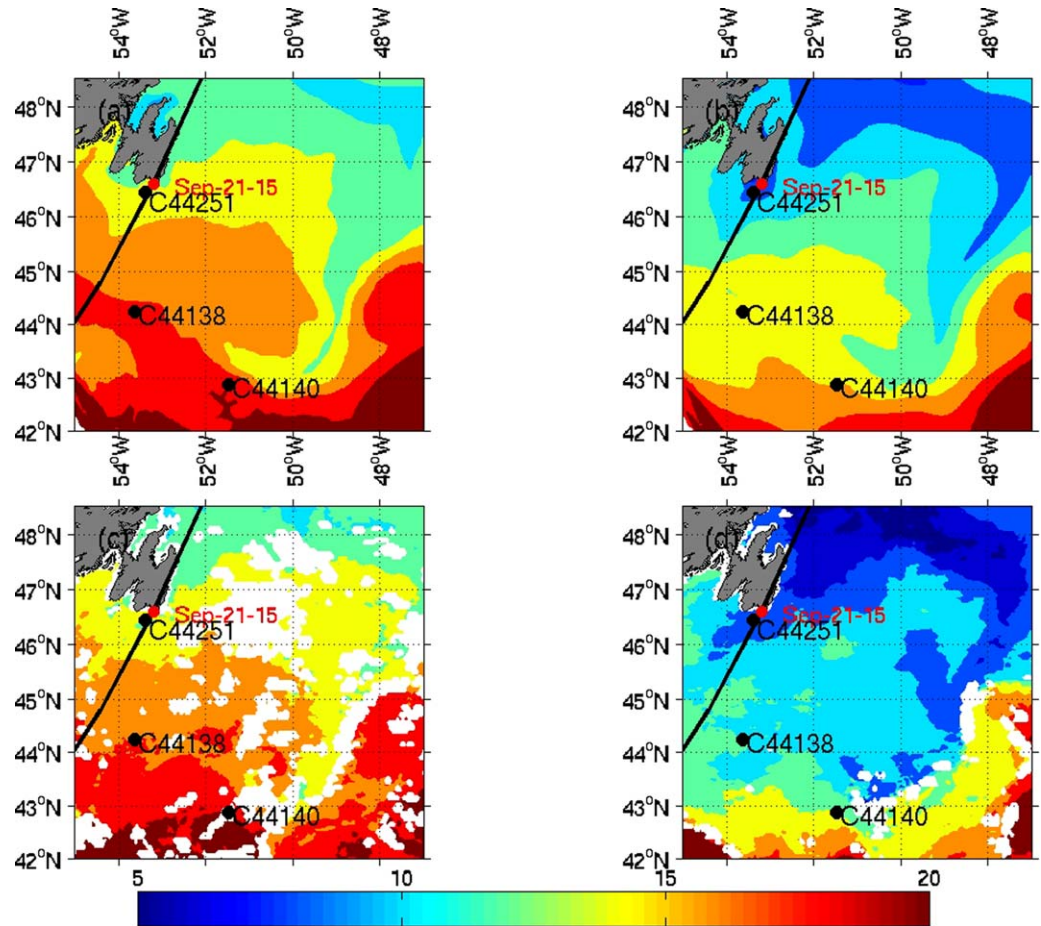


Figure 7. Eight day averaged model sea surface temperature from (a) 14 to 21 September and (b) 22 to 29 September and satellite sea surface temperature from (c) 14 to 21 September and (d) 22 to 29 September. Black line is the Igor track and the black dots are the buoy locations.

slightly lower skills of the 3-D barotropic model. The barotropic model underestimates the observed surge to a greater degree than the baroclinic model, especially at St John’s. This difference may be attributed to the increased bottom current (Figure 10) and thus bottom stress in the 3-D barotropic model. The storm surge, as a temporal and spatial integral of the surface slope, depends strongly on the bottom stress and thus bottom current [Weisberg and Zheng, 2008].

The default turbulence closure for the vertical eddy viscosity/diffusivity in the FVCOM is the 2.5-level Mellor-Yamada turbulence model (MY2.5). Han et al. [2011] reported that the heat flux could not penetrate deep enough when MY2.5 was used in an FVCOM simulation of the seasonal circulation over the Grand Banks. As a result, the model mixed layer depth was too shallow in summer. Thus, we used a second-order $k-\epsilon$ model in GOTM for our baseline simulation in the present study. Here we further compare the model SST during Hurricane Igor from the $k-\epsilon$ and MY2.5 turbulence closures, respectively. Table 3 and Figure 6 clearly show that the model SST change from the $k-\epsilon$ closure agrees well with observations, but that from the MY2.5 closure does not, indicating that the former can realistically represent the mixing effect. The mixed-layer depth from the MY2.5 closure is much shallower than that from the $k-\epsilon$ closure.

As in some previous studies [Morey et al., 2006; Weisberg and Zheng, 2008], we used 1 min sustained hurricane winds as the forcing for the baseline simulation shown in the preceding section. As a comparison the results from a sensitivity run forced by the 10 min sustained hurricane winds were also provided here. Overall, the sensitivity case has larger RMS differences and lower Willmott Score than the baseline model (Table 1) against tide-gauge sea level variations. It underestimates the peak storm surge at all tide-gauge stations (Figure 4 and Table 2). The sensitivity case has essentially the same RMS differences and the

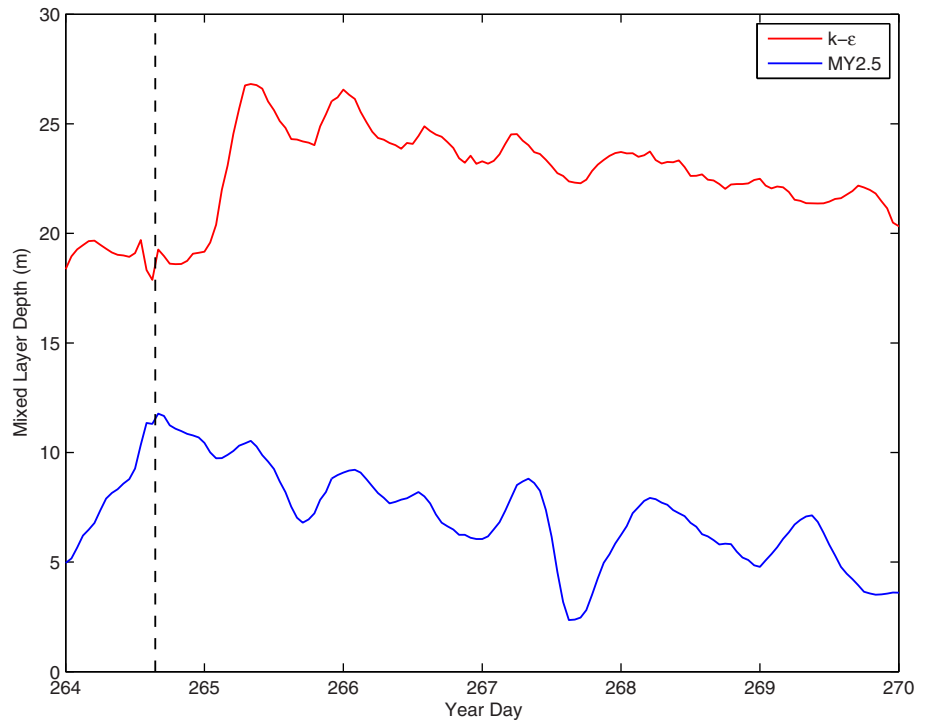


Figure 8. Model mixed-layer depth averaged over an area (from 53 to 54°W and from 46 to 46.5°N) near the inshore buoy location. Black dashed line indicates the landfall time.

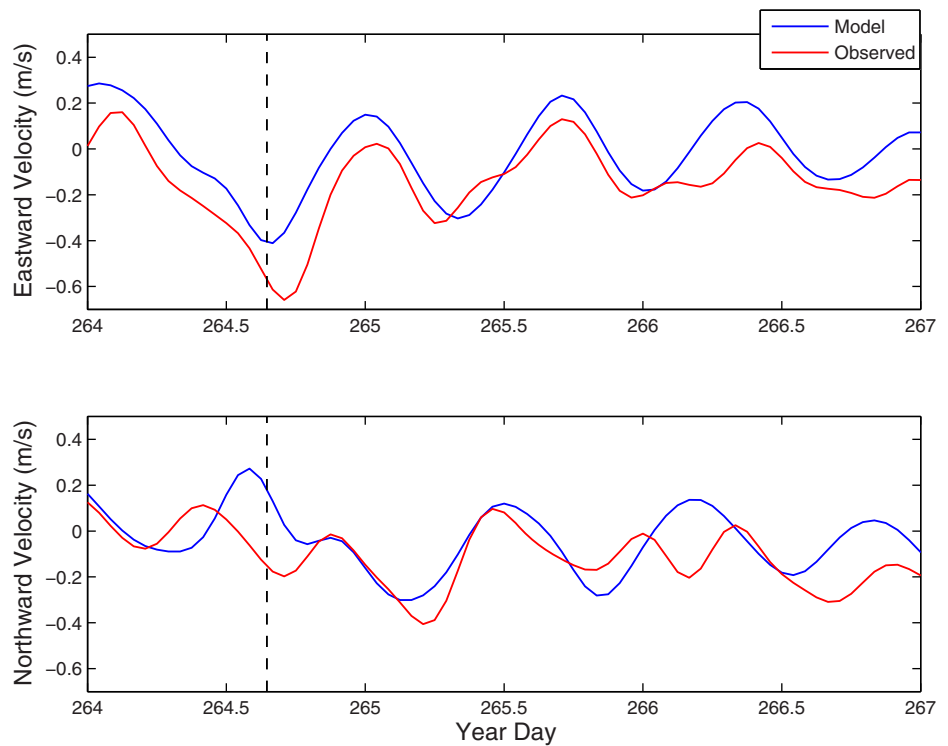


Figure 9. Hourly de-tided near-surface currents at a location (see Figure 1) in the outer Placentia Bay. Blue line is the model surface current while red line is the observed. Black dashed line indicates the landfall time.

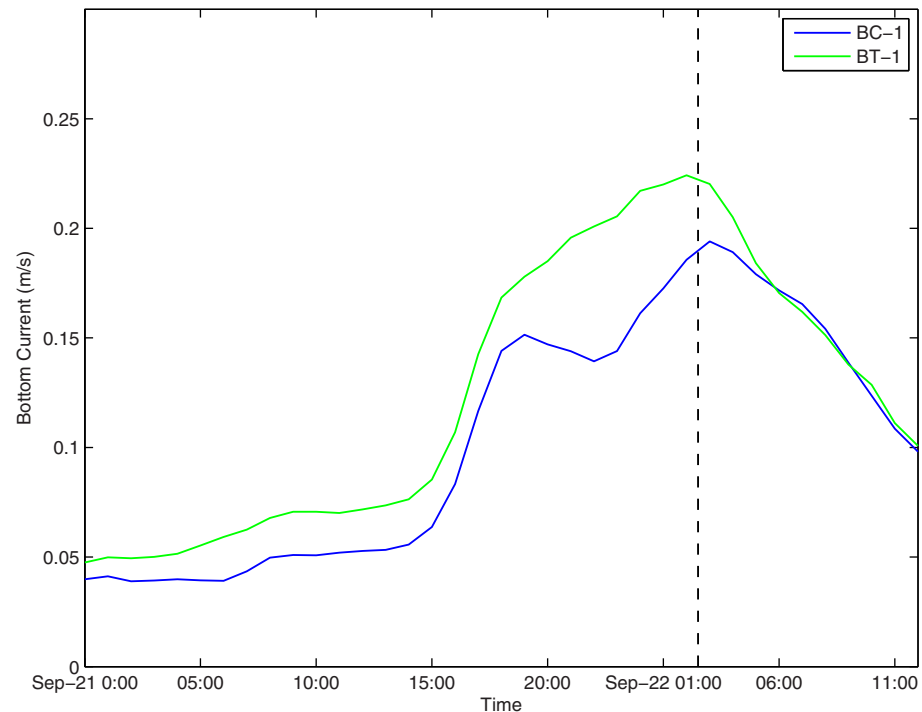


Figure 10. Bottom current speed from the baseline baroclinic model (BC-1) and the sensitivity barotropic case (BT-1), averaged over an area from 52 to 53°W and from 47 to 49°N in the vicinity of St. John's.

Willmott Score against buoy-observed SST (Table 3). The sensitivity case agrees better with observed SST decrease at the nearshore buoy location, but underestimates sea surface cooling at the two offshore buoy locations (Table 3 and Figure 6).

4.2. Sea Level and Continental Shelf Wave

Figure 11a shows the surface circulation pattern and sea level distribution on 21 September (year day 264), 12:00 pm when the storm centre was located at the shelf edge, south of Newfoundland. The winds at this time pushed the water from southern Grand Banks to the coast. Combined with inverse barometric effect, a surge was formed at St. John's, Argentia and St. Lawrence when the storm centre moved close to the Avalon Peninsula (Figure 1) and made landfall. As the storm centre passed the Avalon Peninsula and moved offshore, coastal sea level along the southern coast receded and the winds pushed the water away from the coast toward the outer Grand Banks (Figure 11b). These changes are also seen in the hourly tide gauge data (Figure 4). As the storm traveled farther north, on 22 September (year day 265), 02:00–03:00 (Figures 9c and 9d), the direct storm effects over the Grand Banks became weaker. However, we still observed a significant second surge peak at St. John's at 22 September, 02:40 and at St. Lawrence several hours later.

Both the model solution and observations revealed a stronger second peak at St. John's. In contrast there was only one peak at Bonavista. The source for the second peak can be traced to the higher sea level in Trinity and Conception Bay (Figure 11d). This sea level setup propagated equator-ward along the coast, and caused the second peak surge at St. John's, Argentia and St. Lawrence. To quantify the effect of sea level setup within the two bays, a numerical experiment without them was carried out to examine their impacts on the storm surge magnitude. To do so, the two bay areas were covered with land. The model results without the two bays showed that the second peak at St. John's decreased by 5 cm, but still stronger than the peak at Bonavista. This experiment suggests that the existence of the two bays influenced on the surge magnitude at St. John's. However, the dominant reason to generate the stronger second peak at St. John's is attributed to an inshore Ekman setup when the storm centre was located northeast of St. John's.

Another important feature associated with the storm is the generation and propagation of coastally trapped waves. For example, *Morey et al.* [2006] attributed an anomalously high storm surge along the Florida coast of Apalachee Bay during Hurricane Dennis to a topographic Rossby wave. *Chen et al.* [2014] showed a

Table 3. Sea Surface Temperature Comparison Between Model and Observations at Buoy Locations^a

Buoy Number	RMS Difference (°C)			Willmott Score (WS)			Temperature Decrease (°C)			
	$k-\epsilon-1$	$k-\epsilon-10$	MY2.5-1	$k-\epsilon-1$	$k-\epsilon-10$	MY2.5-1	Model			Obs
							$k-\epsilon-1$	$k-\epsilon-10$	MY2.5-1	
C44140	0.9	1.1	4.2	0.92	0.81	0.35	6.3	4.2	2.7	1.8
C44138	2.4	2.4	6.0	0.67	0.66	0.29	6.3	5.2	4.0	1.8
C44251	1.4	0.6	2.0	0.89	0.97	0.78	5.2	7.5	5.6	2.9
Mean Absolute	1.6	1.4	4.1	0.83	0.81	0.47	5.9	5.6	4.1	2.2

^aThe results shown are from the baseline model ($k-\epsilon-1$), the 10 min sustained wind case ($k-\epsilon-10$), and the MY2.5 turbulence closure (MY2.5-1).

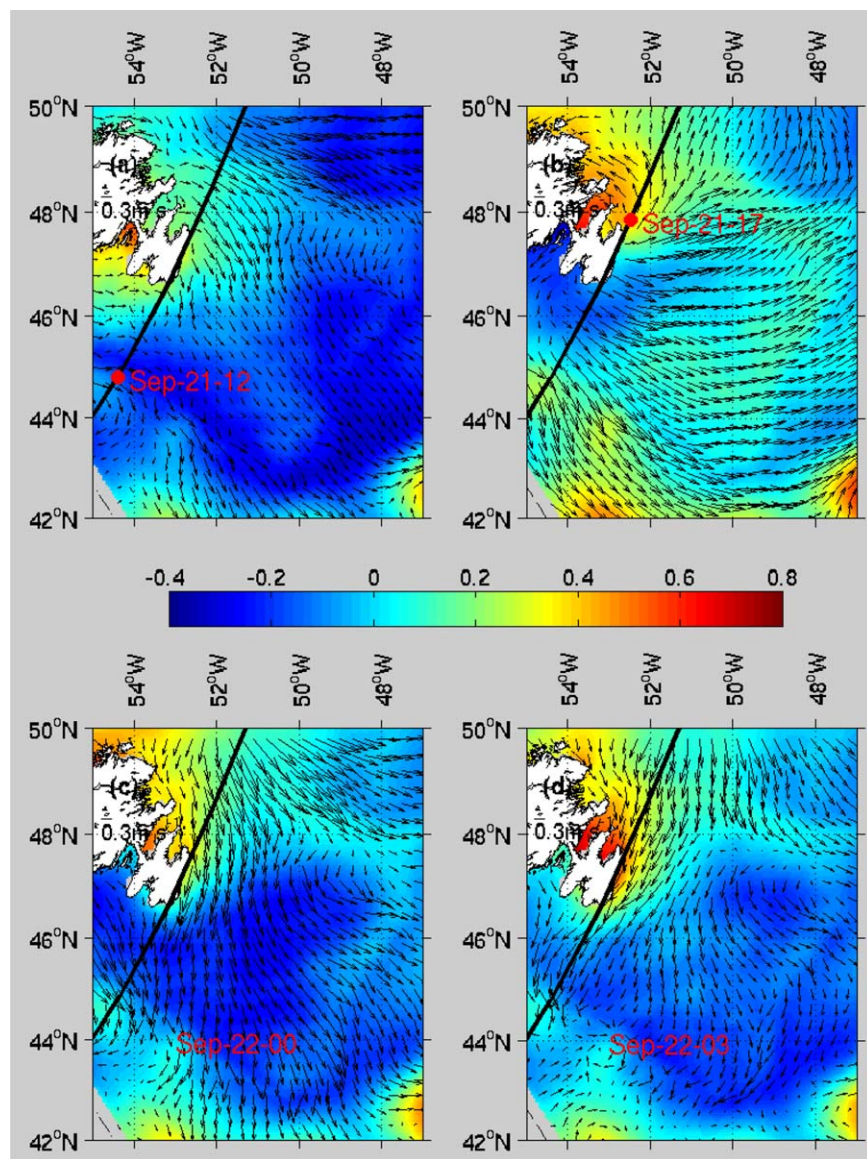


Figure 11. De-tided model surface circulation and sea level distribution at (a) 21 September 12:00 (day 264); (b) 21 September 17:00; (c) 22 September 02:00 (day 265); and (d) 22 September 03:00. Black thick line is the Hurricane Igor track. Red spots are the storm centre at the corresponding time.

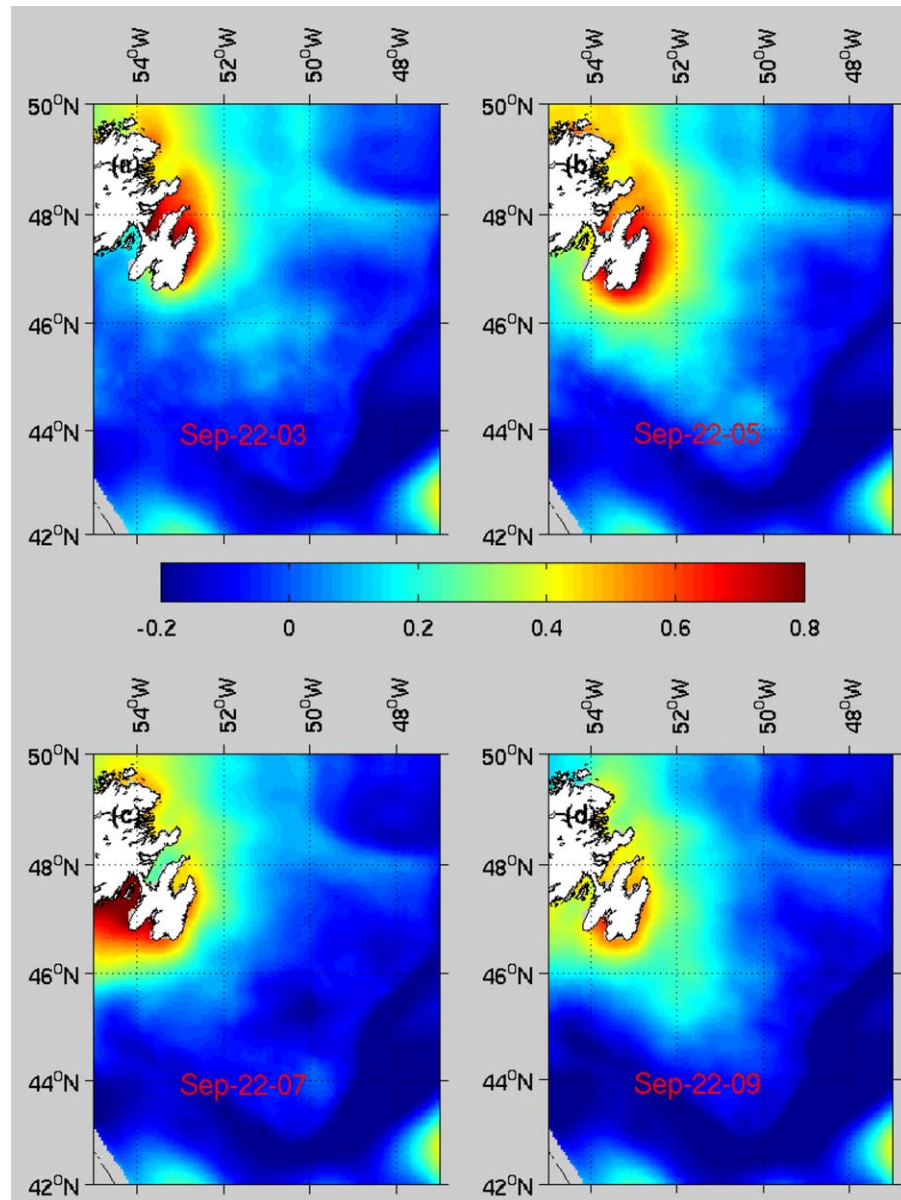


Figure 12. Temporal evolution of the de-tided sea surface elevation (SSE) from the model after the second peak at St. John's at (a) 03:00, (b) 05:00, (c) 07:00, and (d) 09:00 on 22 September (day 265).

continental shelf wave was generated off New Jersey during Hurricane Sandy. *Han et al.* [2012b] suggested the generation of a continental shelf wave when Hurricane Igor passed over the Grand Banks. The propagation of a shelf wave excited by the storm can also be seen from the storm-induced sea surface elevation (Figure 12a). The surface elevation anomaly (Figure 12a) showed a relatively high sea level anomaly in Trinity Bay and Conception Bay at 22 September (year day 265), 03:00. The model showed that this anomaly propagated southward and arrived at St. John's around 22 September 05:00 (Figure 12b). However, the tide-gauge observation at St. John's indicated this high anomaly around 22 September, 02:30. This demonstrated the delay of 2 h in the calculated sea level. At about 22 September, 09:00, the high anomaly left the Placentia Bay to farther west.

To further quantify the storm induced shelf wave we analyzed the observed and simulated sea levels at Bonavista, St. John's and St. Lawrence. The time period is from 23 September, 01:30 to 27 September, 01:30, 2010, the same as that used in *Han et al.* [2012b]. Observed post-storm sea level indicates that the dominant period of oscillation is 48 h or 0.5 cycle per day (cpd) at St. John's. A similar oscillation was also found at St.

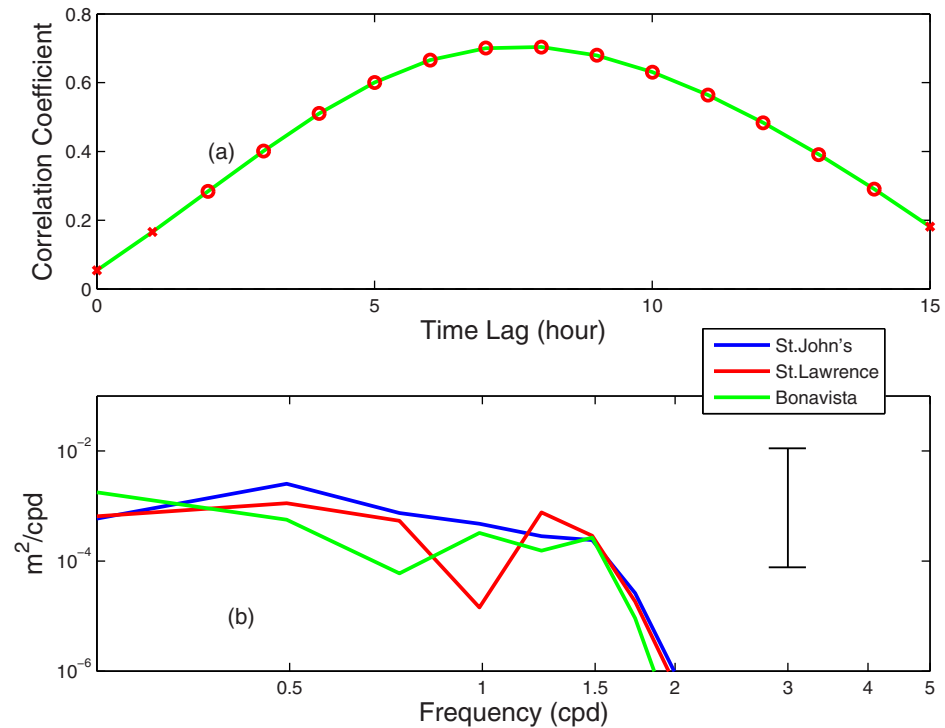


Figure 13. (a) Lagged correlation coefficients (open circles: significantly different from zero at the 99% confidence level; cross: insignificant) between the tide-gauge sea level anomalies at St. John's and St. Lawrence, with the latter lagging the former. (b) Power spectral density of the tide-gauge sea level anomalies at St. John's, Bonavista and St. Lawrence, along with the 95% confidence interval (vertical bar).

Lawrence, but not at Bonavista. Sea level at St. Lawrence lags that at St. John's by 7–8 h. The propagation speed of sea level is estimated to be 14–16 m/s (Figure 13a), consistent with previous results for the Canadian Atlantic shelves based on the numerical model and sea level observations [Tang *et al.*, 1998; Sheng *et al.*, 2006; Thiebaut and Vennell, 2010; Han *et al.*, 2012b]. Han *et al.* [2012b] estimated the averaged shelf-wave speed to be ~ 10 m/s. Compared with the observations, our model results show similar wave characteristics both in the propagation speed and wave frequency (Figure 14). Some difference was observed at St. Lawrence where the model frequency was 0.7 cpd.

Overall, the simulated sea level agrees well with observations in the subinertial band. After separating the high- and low-frequency signals of sea level at St. John's bounded by the inertial frequency, we found that the correlation coefficient between observed and model results was 0.8 for the subinertial band; but insignificant for the other band. Similarly, Bonavista and St. Lawrence stations had high correlation in the subinertial frequency. Thus, the model and observed sea level difference is mainly in the high-frequency band above the inertial frequency, which is in part associated with uncertainty in representing the storm high frequency wind forcing.

By analysing the time series of model depth-averaged current at a location off St. Lawrence (Figure 1), the storm-induced free-wave oscillations were also examined. The magnitude of the depth-averaged horizontal current speed at this location reached 20 cm/s during the storm period (Figure 15). The oscillation had a dominant period of about 0.7 cpd (Figure 15b), consistent with that of the sea level oscillation at the same location (Figure 13d).

4.3. Entrainment and Upwelling

Price [1981] and Wada [2005] suggest the sea surface cooling during the hurricane is primarily caused by entrainment and upwelling. These papers also introduce two nondimensional numbers: the Burger Number and the Rossby number, to demonstrate the evolution of storm effects on surface cooling. Here we follow their definition for the Burger number (B):

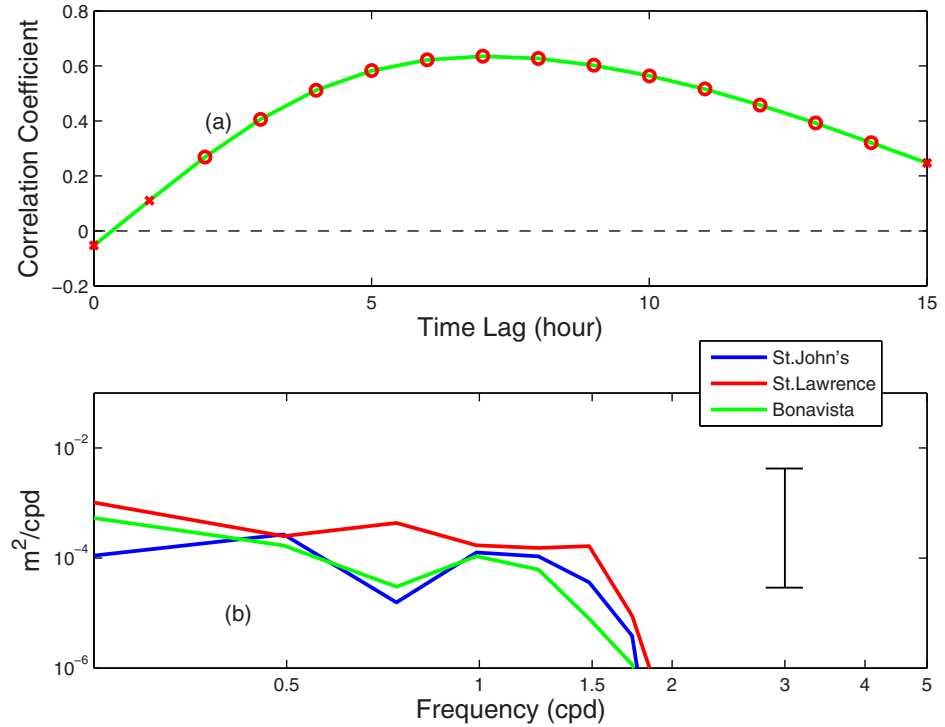


Figure 14. (a) Lagged correlation coefficients (open circles: significantly different from zero at the 99% confidence level; cross: insignificant) between the model sea level anomalies at St. John's and St. Lawrence, with the latter lagging the former. (b) Power spectral density of the model sea level anomalies at St. John's, Bonavista and St. Lawrence, along with the 95% confidence interval (vertical bar).

$$B = \frac{g' h_l}{4f^2 R_{\max}^2} \quad (5)$$

where g' is the reduced gravity and h_l is the mixed layer depth after cooling. The Burger number represents the scale of turbulent mixing. We first determine the mixed-layer depth. The difference between the mixed-layer density and that in the rest of water column is used to calculate the reduced gravity. Instead of the Rossby number, we introduce an Ekman Pumping Index (E):

$$E = \frac{\text{curl}(\vec{\tau})}{\rho_o U_H f} \quad (6)$$

where U_H is the storm translation speed. We calculated the Burger number and the Ekman Pumping Index from the model results at the inshore buoy location (C44251, Figure 1).

When the storm centre was approaching to Newfoundland in the morning of 21 September, the ocean was well stratified, with a large Burger number (Figure 16a). One to 2 h before landfall, the Ekman upwelling effect started to pump colder water from subsurface. The turbulent mixing also picked up. Thus the density difference between the mixed layer and the lower water column decreased and the Burger number began to fall. At 15:00, the turbulent mixing and upwelling effects reached the sea surface and SST started to fall. The Ekman upwelling weakened at 16:00 (Figure 16b). The SST fell by about 2°C from 15:00 to 17:00. While the Burger number continued to fall, the SST fall paused for 2–3 h. Afterward, SST fell again together with the Burger number. The SST adjustment ended at 03:00 22 September, while the Burger number did not end until 5 h later. When the MY2.5 turbulence closure is used, the Burger number is much lower and shows little change during the storm.

Although the Burger number and Ekman pumping index show when turbulent entrainment and Ekman upwelling take place, they do not provide information on their relative importance. The two processes both contribute to sea surface cooling but their influences on the mixed-layer depth are opposite. The former deepens it and the latter uplifts it. We have calculated the Ekman pumping velocity and cumulative

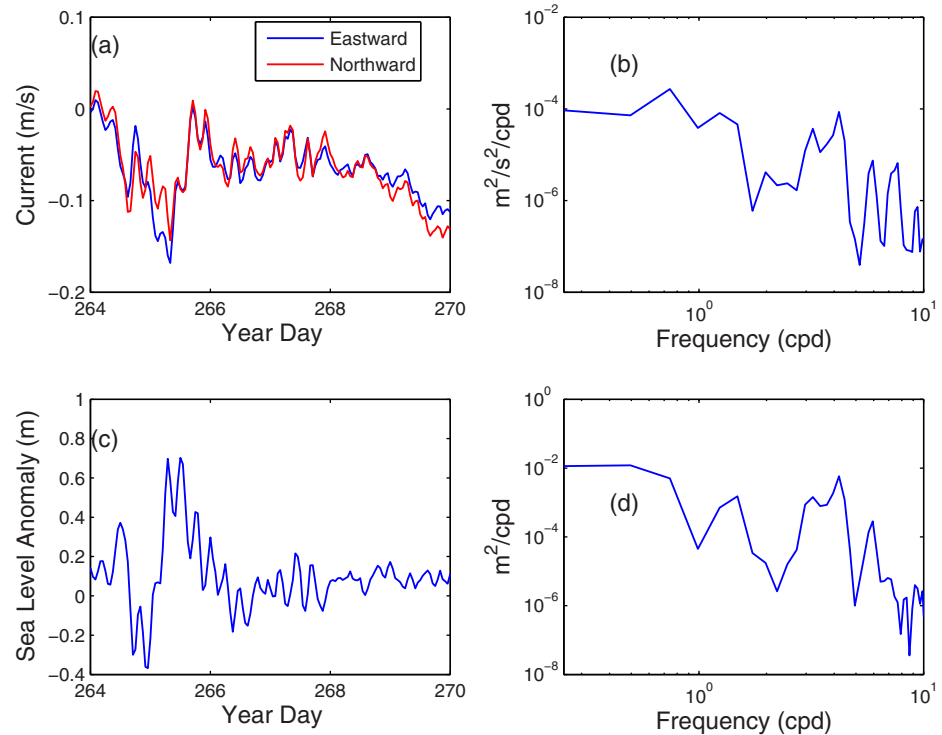


Figure 15. (a) Vertically averaged current at a location indicated in Figure 1 and (b) its power spectral density of the total current speed. (c) Sea level anomaly and (d) Power spectral density.

distance for an area around the buoy location (Figures 16c and 16d). The net cumulative upwelling distance is estimated to be 5 m. With the simulated mixed-layer deepening of about 8 m, the turbulent entrainment deepened the mixed-layer by 13 m. Therefore, the turbulent entrainment is the dominant process over the Ekman upwelling in inducing the sea surface cooling.

5. Conclusion

A 3-D, baroclinic, finite-volume ocean model was developed to study the upper ocean responses to Hurricane Igor over the Grand Banks of Newfoundland. Reconstructed hurricane winds were applied to force this ocean model to explore the dynamics of midlatitude coastal waters.

The 3-D baroclinic ocean model reproduced the sea surface elevation before and after the storm reasonably well. Especially, the two surges generated by the passage of Hurricane Igor were well captured. Both the model and observations showed two surges at St. John's, Argentia and St. Lawrence. The first surge was attributed to the direct local wind forcing and the second one was the result of the equator-ward propagating continental shelf wave generated by the storm. Compared with hourly observations, the model sea surface elevation had an RMS error of 10 cm on average from day 264 to 270. The model underestimates storm surge magnitude at St. John's and Bonavista. The model overestimation of the surge at Argentia and St. Lawrence is related to storm-induced seiche which seems not well captured by tide-gauge observations. For the highest surges, the average model-observation magnitude difference was 8 cm, with a model time lag within 1.3 h. Sea level at the three stations was separated into high- and low-frequency components bounded by the inertial frequency for further analysis, which indicates poor and good agreement with observations for the former and latter respectively. In the future, by applying the observed hourly and high-resolution wind data in the hurricane model [Rego and Li, 2010], we should improve the reconstructed local winds so that the ocean model could generate more accurate high-frequency sea level.

The model surface temperatures were compared with observations at three buoy stations over the Grand Banks. Both model and observation showed a significant decrease about 6°C in the sea surface temperature. The RMS difference between the model and observation from day 264 to day 270 was about 1.6°C .

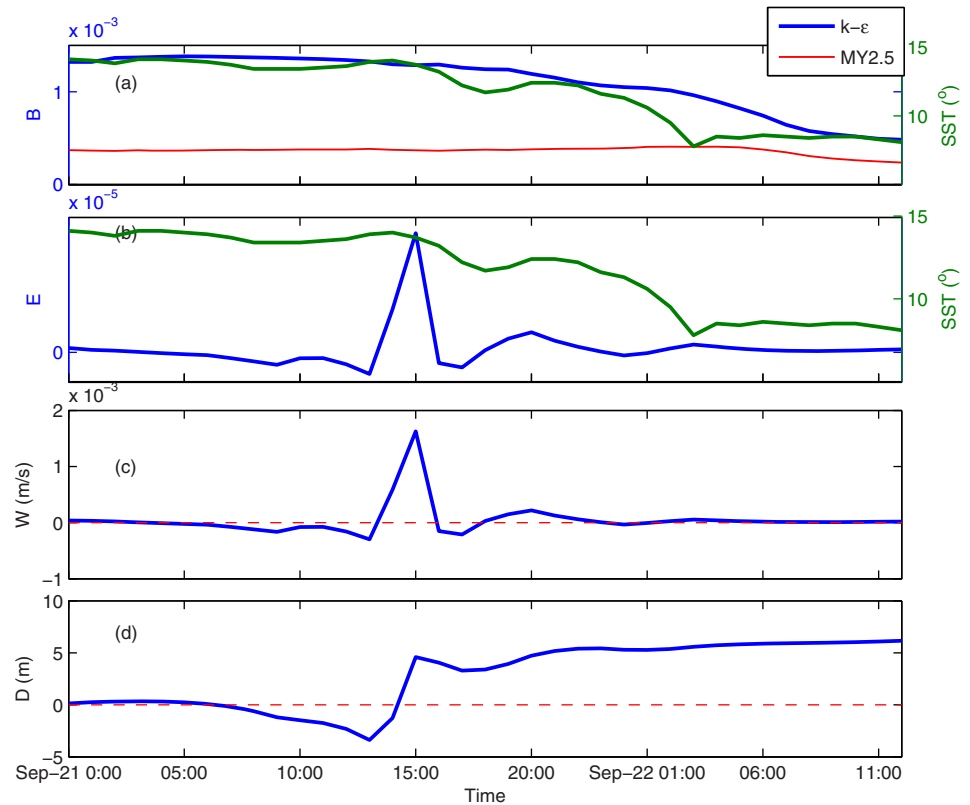


Figure 16. Time series of (a) the Burger Number B , (b) the Ekman Pumping Index E , (c) Ekman upwelling velocity W , and (d) Cumulative upwelling distance D at the inshore buoy location (C44251, see Figure 1). The observed sea surface temperature (SST, green curve) is also shown in (a) and (b).

Furthermore, the calculated horizontal distribution of the sea surface temperature was compared with satellite observations. The model reproduced well the southward increase of temperature observed before the storm and the sharp decrease afterward.

The model sea surface current was compared with observations at a point located in the outer Placentia Bay. The correlation coefficient between the model and observations was 0.7. The model was able to generate the observed variability of surface currents. In particular when the storm passed over Newfoundland, the calculated surface currents well captured the strong southwestward flow of 0.7 m/s.

The storm induced shelf wave was examined by analysing the sea level at tide-gauge stations and currents at a point far away from the storm centre to prevent direct storm wind effects. Both observation and model results showed a propagation speed of 14–16 m/s and 0.5–0.7 CPD, consistent with the continental shelf-wave estimation from *Han et al.* [2012b]. We further analyzed the vertically averaged currents in the outer Placentia Bay. The results highly support those from sea level data. The storm excited waves propagate equatorward along the Newfoundland coast. These waves can not only be observed from the sea surface elevation field but also from the horizontal currents.

An examination of Burger number and Ekman pumping parameters indicates that the entrainment due to turbulent mixing is the dominant process to cause the salient drop in SST. Upwelling associated with the wind stress curl plays a small supplementary role only.

The present study provides new insights into simulating ocean’s response to hurricanes. It is found that a 3-D baroclinic model simulates storm surge slightly better than an alternative 3-D barotropic model. The difference may be attributed to smaller bottom current and thus friction in the 3-D baroclinic model. It is shown that sea surface cooling is well simulated with a $k-\epsilon$ turbulence closure, but is significantly underestimated with the commonly used MY2.5 closure.

Acknowledgments

The work was partially supported by the Centre for the Ocean Model Development and Application, Fisheries and Oceans Canada. We thank Changsheng Chen for providing the FVCOM code and three anonymous reviewers for their useful comments. The tide-gauge data and buoy SST data are from the Integrated Science Data Management, Fisheries and Oceans Canada. The buoy currents data are the Smart Bay Project, Newfoundland and Labrador. The atmospheric forcing data are from NCEP Reanalysis data provided by the NOAA/OAR/ESRL PSD, Boulder, Colorado, USA, from their Web site at <http://www.esrl.noaa.gov/psd/>. The satellite SST data are from the Pathfinder Project, NOAA. The online links to all these data are provided in the manuscript.

References

- Casey, K. S., T. B. Brandon, P. Cornillon, and R. Evans (2010), The past, present and future of the AVHRR Pathfinder SST program, in *Oceanography from Space: Revisited*, edited by V. Barale, J. F. R. Gower, and L. Alberotanza, pp. 273–288, Springer, N. Y., doi:10.1007/978-90-481-8681-5_16.
- Chen, C., H. Liu, and R. C. Beardsley (2003), An unstructured grid, finite volume primitive equation coastal ocean model: Application to coastal ocean and estuaries, *J. Atmos. Oceanic Technol.*, *20*, 159–186.
- Chen, C., et al. (2011), An Unstructured Grid Finite-Volume Coastal Ocean Model (FVCOM) System. FVCOM User Manual, 3rd ed. Massachusetts Institute of Technology, Cambridge, Mass.
- Chen, N., G. Han, J. Yang, and D. Chen (2014), Hurricane Sandy storm surges observed by HY-2A satellite altimetry and tide gauges, *J. Geophys. Res. Oceans*, *119*, 4542–4548, doi:10.1002/2013JC009782.
- deYoung, B., and C. Tang (1990), Storm-forced baroclinic near-inertial currents on the Grand Bank, *J. Phys. Oceanogr.*, *20*, 1725–1741.
- Fairall, C. W., E. F. Bradley, D. P. Rogers, J. B. Edson, and G. S. Young (1996), Bulk parameterization of air-sea fluxes for COARE, *J. Geophys. Res.*, *101*, 3747–3764.
- Foreman, M., P. Czajko, D. J. Stucchi, and M. Guo (2009), A finite volume model simulation for the Broughton Archipelago, Canada, *Ocean Modell.*, *30*, 29–47.
- Fung, I. Y., D. E. Harrison, and A. A. Lacis (1984), On the variability of the net long-wave radiation at the ocean surface, *Rev. Geophys.*, *22*, 177–193.
- Geshelin, Y., J. Sheng, and R. J. Greatbatch (1999), Monthly mean climatologies of temperature and salinity in the western North Atlantic, *Can. Tech. Rep. Hydrogr. Ocean Sci. Rep.* 153, Ocean Sci. Div. of Fish. and Ocean Can., Dartmouth, Nova Scotia, Canada.
- Han, G., Z. Lu, Z. Wang, J. Helbig, N. Chen, and B. deYoung (2008), Seasonal variability of the Labrador Current and shelf circulation off Newfoundland, *J. Geophys. Res.*, *113*, C10013, doi:10.1029/2007JC004376.
- Han, G., S. Paturi, B. deYoung, S. Yi, and C. K. Shum (2010), A 3-D data assimilative tide model of Northwest Atlantic, *Atmos. Ocean*, *48*, 39–57.
- Han, G., Z. Ma, B. deYoung, M. Foreman, and N. Chen (2011), Simulation of three-dimensional circulation and hydrography over the Grand Banks of Newfoundland, *Ocean Modell.*, *40*, 199–210, doi:10.1016/j.ocemod.2011.08.009.
- Han, G., Z. Ma, and N. Chen (2012a), Hurricane Igor impacts on the stratification and phytoplankton bloom over the Grand Banks, *J. Mar. Syst.*, *100–101*, 19–25.
- Han, G., Z. Ma, D. Chen, B. deYoung, and N. Chen (2012b), Observing storm surges from space: Hurricane Igor off Newfoundland, *Sci. Rep.*, *2*, doi:10.1038/srep01010.
- Holland, G. J. (1980), An analytic model of the wind and pressure profiles in hurricanes, *Mon. Weather Rev.*, *108*, 212–218.
- Jones, J. E., and A. M. Davies (2004), On the sensitivity of computed surges to open-boundary formulation, *Ocean Dyn.*, *54*(2), 142–162.
- Large, W. G., and S. Pond (1981), Open ocean momentum fluxes in moderate to strong winds, *J. Phys. Oceanogr.*, *11*, 324–336.
- Li, J., J. Scinocca, J. Lazare, M. McFarlane, N. McFarlane, K. Von Salzen, and L. Solheim (2006), Ocean surface albedo and its impact on radiation balance in climate model, *J. Clim.*, *19*, 6314–6333.
- Liu, Y., P. MacCready, B. M. Hickey, E. P. Dever, P. M. Kosro, and N. S. Banas (2009), Evaluation of a coastal ocean circulation model for the Columbia River plume in summer 2004, *J. Geophys. Res.*, *114*, C00B04, doi:10.1029/2008JC004929.
- Ma, Z., G. Han, and B. deYoung (2012), Modelling temperature, currents and stratification in Placentia Bay, *Atmos. Ocean*, *50*, 244–260, doi:10.1080/07055900.2012.677413.
- Mercer, D., J. Sheng, R. J. Greatbatch, and J. Bobanovic (2002), Barotropic waves generated by storms moving rapidly over shallow water, *J. Geophys. Res.*, *107*(C10), 3152, doi:10.1029/2001JC001140.
- Mellor, G. L., T. Ezer, and L. Y. Oey (1993), The pressure gradient conundrum of sigma coordinate ocean models, *J. Atmos. Oceanic Technol.*, *11*, 1126–1134.
- Monahan, E. G., and G. MacNiocaill (1986), *Oceanic Whitecaps and Their Role in Air-Sea Exchange Processes*, Springer, N. Y.
- Morey, S. L., S. Baig, M. A. Bourassa, D. S. Dukhovskoy, and J. J. O'Brien (2006), Remote forcing contribution to storm-induced sea level rise during Hurricane Dennis, *Geophys. Res. Lett.*, *33*, L19603, doi:10.1029/2006GL027021.
- Pasch, R. J., and T. B. Kimberlain (2011), Tropical Cyclone Report Hurricane Igor (AL112010), National Hurricane Center, Fla.
- Pawlowicz, R., B. Beardsley, and S. Lentz (2002), Classical tidal harmonic analysis including error estimates in MATLAB using T_TIDE, *Comput. Geosci.*, *28*, 929–937.
- Peng, M., L. Xie, and J. Pietrafesa (2006a), A numerical study on hurricane induced storm surge and inundation in Charleston, South Carolina, *J. Geophys. Res.*, *111*, C08017, doi:10.1029/2004JC002755.
- Peng, M., L. Xie, and J. Pietrafesa (2006b), Tropical cyclone induced asymmetry of sea level surge and fall and its presentation in a storm surge model with parametric wind fields, *Ocean Modell.*, *14*, 81–101.
- Phadke, A. C., C. D. Martino, K. F. Cheung, and S. H. Houston (2003), Modelling of tropical cyclone winds and waves for emergency management, *Ocean Eng.* *30*, 553–578.
- Price, F. (1981), Upper ocean response to a hurricane, *J. Phys. Oceanogr.*, *11*, 153–175.
- Rego, J. L., and C. Li (2010), Storm surge propagation in Galveston Bay during Hurricane Ike, *J. Mar. Syst.*, *82*, 265–279.
- Resio, D. T., and J. J. Westerink (2008), Modeling the physics of storm surges, *Phys. Today*, *61*(9), 33–38.
- Shen, J., W. Gong, and H. V. Wang (2006), Water level response to 1999 Hurricane Floyd in the Chesapeake Bay, *Cont. Shelf Res.*, *26*, 2484–2502.
- Sheng, J., X. Zhai, and R. Greatbatch (2006), Numerical study of storm-induced circulation on the Scotian Shelf during Hurricane Juan using a nested-grid ocean model, *Prog. Oceanogr.*, *70*, 233–254.
- Tang, C. L., Q. Gui, and B. M. Detrayce (1998), Barotropic response of the Labrador/Newfoundland Shelf to a moving storm, *J. Phys. Oceanogr.*, *28*, 1152–1172.
- Thiebaud, S., and R. Vennell (2010), Observation of a fast continental shelf wave generated by a storm impacting Newfoundland using wavelet and cross-wavelet analyses, *J. Phys. Oceanogr.*, *40*, 417–428.
- Wada, A. (2005), Numerical simulations of sea surface cooling by a mixed layer model during the passage of Typhoon Rex, *J. Oceanogr.*, *61*, 41–57.
- Weisberg, R. H., and L. Zheng (2006a), Hurricane storm surge simulation for Tampa Bay, *Estuaries Coasts*, *29*(6), 899–913.
- Weisberg, R. H., and L. Zheng (2006b), A simulation of the Hurricane Charley storm surge and its breach of North Captiva Island, *Fla. Scientist*, *69*, 152–165.
- Weisberg, R. H., and L. Zheng (2008), Hurricane Storm surge simulations comparing three-dimensional with two-dimensional formulations based on an Ivan-like storm over the Tampa Bay, Florida region, *J. Geophys. Res.*, *113*, C12001, doi:10.1029/2008JC005115.

- Westerink, J. J., R. A. Luettich, J. C. Feyen, J. H. Atkinson, C. Dawson, H. J. Roberts, M. D. Powell, J. P. Dunion, E. J. Kubatko, and H. Pourtaheri (2008), A basin- to channel-scale unstructured grid hurricane storm surge model applied to Southern Louisiana, *Mon. Weather Rev.*, *136*, 833–864.
- Willmott, C. J. (1981), On the validation of models, *Phys. Geogr.*, *2*, 184–194.
- Xie, L., L. Pietrafesa, and M. Peng (2004), Incorporation of a mass-conserving inundation scheme into a three dimensional storm surgemodel, *J. Coastal Res.*, *20*(4), 1209–1223.
- Zhang, J. A., and E. W. Uhlhorn (2012), Hurricane sea surface inflow angle and an observation-based parametric model, *Mon. Weather Rev.*, *140*, 3587–3605.